Article

Femtosecond Laser Ablation-Induced Magnetic Phase Transformations in FeRh Thin Films

Pavel Varlamov [1,*], Anna Semisalova [2,*], Anh Dung Nguyen [3], Michael Farle [2], Yannis Laplace [1], Michele Raynaud [1], Olivier Noel [3], Paolo Vavassori [4,5] and Vasily Temnov [1,*]

1   LSI, Ecole Polytechnique, CEA/DRF/IRAMIS, CNRS, Institut Polytechnique de Paris, 91128 Palaiseau, France
2   Faculty of Physics and CENIDE, University of Duisburg-Essen, 47057 Duisburg, Germany
3   Institut des Molécules et Matériaux du Mans—UMR 6283 CNRS, Le Mans Université, 72085 Le Mans, France
4   CIC nanoGUNE—BRTA, Donostia—San Sebastian, 20018 Donostia, Spain
5   IKERBASQUE, Basque Foundation for Science, 48009 Bilbao, Spain
*   Correspondence: pavel.varlamov@polytechnique.edu (P.V.); anna.semisalova@uni-due.de (A.S.); vasily.temnov@cnrs.fr (V.T.)

Abstract: In this study, we present a novel investigation into the magnetic and morphological properties of equiatomic B2-ordered FeRh thin films irradiated with single high-intensity ultrashort laser pulses. The goal is to elucidate the effect of femtosecond laser ablation on the magnetic properties of FeRh. We employed Scanning Magneto-Optical Kerr Effect (S-MOKE) microscopy to examine the magnetic phase after laser processing, providing high spatial resolution and sensitivity. Our results for the first time demonstrated the appearance of a magneto-optical signal from the bottom of ablation craters, suggesting a transition from antiferromagnetic to ferromagnetic behavior. Fluence-resolved measurements clearly demonstrate that the ablation threshold coincides with the threshold of the antiferromagnet-to-ferromagnet phase transition. The existence of such a magnetic phase transition was independently confirmed by temperature-dependent S-MOKE measurements using a CW laser as a localized heat source. Whereas the initial FeRh film displayed a reversible antiferromagnet-ferromagnet phase transition, the laser-ablated structures exhibited irreversible changes in their magnetic properties. This comprehensive analysis revealed the strong correlation between the femtosecond laser ablation process and the magnetic phase transformation in FeRh thin films.

Keywords: FeRh films; femtosecond laser pulse; laser ablation; S-MOKE microscopy; antiferromagnetism; ferromagnetism

1. Introduction

Magnetic properties of matter and their control by external stimuli play a crucial role in various fields such as information storage, spintronics, and energy conversion. The behavior of materials, i.e., magnetic susceptibility, depends on the arrangement of their magnetic moments, leading to different types of magnetic phases, such as ferromagnetic (FM), antiferromagnetic (AF), and paramagnetic (PM).

One of the easiest ways to induce magnetic phase transition is to increase the temperature, leading to the FM-to-PM transitions followed by the Curie–Weiss law [1]. An elegant way to locally heat the material is provided by focusing a beam of continuous or pulsed laser radiation on the sample surface. The pulsed laser excitation of magnetic materials offers the design of various magnetic phenomena as a function of the absorbed laser energy per unit area, the so-called laser fluence. For example, after applying femtosecond laser pulses at low absorbed fluences, the phenomenon of ultrafast demagnetization induced by the rapid increase of the spin temperature was observed by J.-Y. Bigot on the subpicosecond timescale [2]. At longer picosecond-to-nanosecond time scales, it is possible to observe

and quantify the precessional magnetization dynamics induced by thermal [3–5] and/or acoustic transients [6–9].

At higher laser fluences, but still below the laser damage threshold, it was readily possible to achieve irreversible changes in magnetic properties. For instance, Kisielewski et al. investigated magnetic phases in Pt/Co/Pt multilayers after irradiation with single and multiple femtosecond laser pulses [10]. At fluences below the ablation threshold, the magnetization could be switched from an in-plane to an out-of-plane state. Increasing the number of applied pulses led to a more extensive modification of regions with switched magnetization [10].

Irreversible changes in magnetic properties have also been explored in more complex materials. Back in 1981, Urner-Wille et al. demonstrated the formation of regions with distinct hysteresis loop shapes after irradiating amorphous GdFeBi films with a single picosecond pulse [11]. More recent investigations on B2-ordered $Fe_{60}Al_{40}$ revealed the possibility of switching to a ferromagnetic state after the laser-induced melting of the material [12,13]. The authors attributed this observation to a chemical order–disorder phase transition in the crystal lattice [14,15] due to laser-induced melting and rapid resolidification. Subsequent treatment with a lower-intensity laser pulse allowed for the "erasure" of the ferromagnetic state [12]. Magnetization reversal was also achieved in GdFeCo films due to irradiation with circularly polarized femtosecond pulses [16,17]. The switching phenomenon (Faraday effect), which was originally interpreted as the coherent helicity-dependent phenomenon, appeared to be fine-tuned through the small (∼1%) difference in the absorbed laser fluence due to the magneto-circular dichroism, i.e., of purely thermal nature [18]. This example demonstrates the sharp threshold in the absorbed laser fluence for ultrafast laser-induced phase transitions.

Another interesting complex magnetic material is the binary alloy FeRh which exhibits FM, AF, and PM state, depending on its temperature, composition and a structural order [19–21]. Specifically, at the nearly equiatomic concentration, B2-FeRh exhibits AF ordering at room temperature with a transition to FM ordering at around 370 K [19]. The transition temperature is sensitive to stoichiometry and structural disorder [22,23]. This unique tunability has generated significant interest in FeRh for applications such as magnetic memory [19,24,25] and magnetocaloric cooling [26–28].

Modifications by doping or by applying strain on FeRh can also cause changes in its magnetization behavior [29–33]. Numerous studies demonstrated that an irreversible magnetostructural phase transition can be induced in FeRh by ion beam irradiation; additionally, varying the fluence of irradiation can be used to tune the phase transition temperature [23,34–38] as well as to induce a formation of fcc-FeRh phase [20]. In contrast, the laser excitation of FeRh was studied only with low-intensity pulses to generate ferromagnetic order on subpicosecond timescales [39–42].

In this paper, we discuss the magnetic properties of FeRh after irradiation with a single fs pulse at high intensities. Scanning MOKE (S-MOKE) microscopy was employed to investigate the magnetic phase after laser processing, offering high spatial resolution and sensitivity. A magneto-optical signal was observed inside the ablated film following the laser irradiation. An analysis of the signal amplitudes as a function of fluence suggests that the initiation of the ablation is responsible for the appearance of the magneto-optical signal. Subsequent S-MOKE measurements during heating under ambient atmosphere up to T > 600 K revealed the reversible temperature-driven AF-FM phase transition of the initial B2-ordered film, while the magneto-optical signal in the ablated regions has been erased by this heat treatment.

2. Materials and Methods

First, 45 nm thick films of equiatomic FeRh were sputter-deposited from an alloyed target on MgO(001) substrate at 600 °C. Prior to deposition, the substrate was annealed at 600 °C for 8 h; after deposition, the FeRh film was kept at 600 °C for two hours to achieve the B2-ordered structure. The base pressure of the vacuum chamber was 3×10^{-7} mbar (3×10^{-7} hPa), sputtering was performed in Ar atmosphere at

5.5×10^{-3} mbar (5.5×10^{-3} hPa) pressure. Next, the laser nanostructuring was completed under an ambient atmosphere. A train of the laser pulses (800 nm wavelength, 50 fs duration, 500 Hz repetition rate, pulse energy up to 300 µJ) was focused by a quartz lens (F = 40 cm) into the beam waist of ω_0 = 30 µm under 45°. During the irradiation, the sample was moving at a constant speed (10 cm/s), which allowed producing identical fs-laser-induced structures. Surface characterizations were performed using a Bruker DI 3100 (Nanoscope V) atomic force microscope (AFM).

After the irradiation, we utilized magneto-optical Kerr effect (MOKE) microscopy to study the magnetic properties of the produced structures at room temperature. Figure 1 illustrates the setup. The transversal MOKE configuration (T-MOKE, magnetization is perpendicular to the plane of polarization) was employed for measurements, focusing on the ratio of the reflected intensity change (ΔI) in the magnetic field to the initial reflected intensity (I_0), i.e., $\Delta I / I_0$. We used a p-polarized collimated laser beam, with a wavelength of 632.8 nm, as the incident light. This beam was then diverged with a lens and focused into a 2 µm spot using a 10× microscope. The reflected beam was focused on the windows of the photodetector with a different lens. The sample was placed in an oscillating magnetic field ($m_x = \pm 1$) of 50 mT at 1.5 kHz.
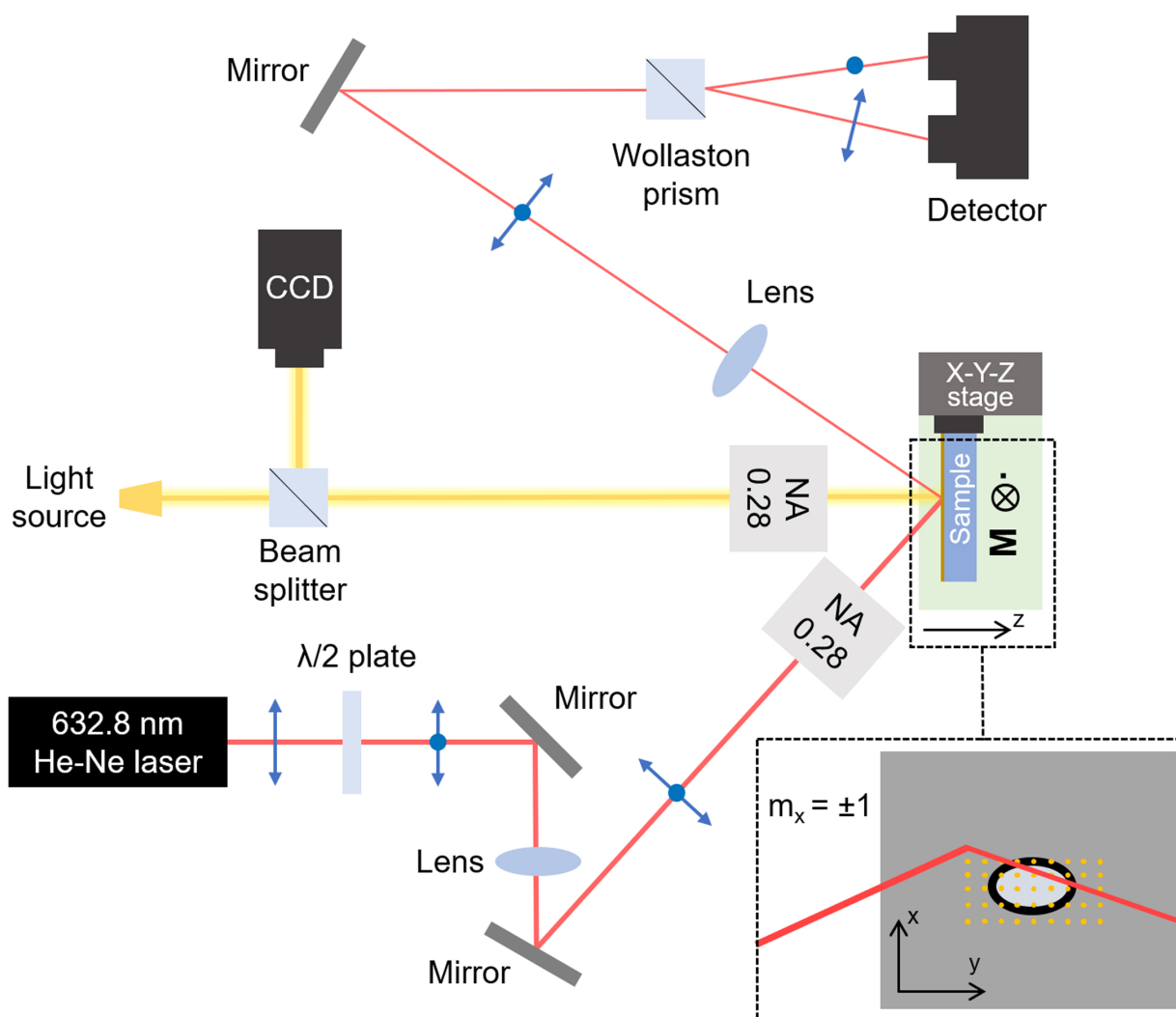
Figure 1. Schematics of the setup for the S-MOKE microscopy in the transversal MOKE configuration with balanced photodetection using polarized light. m_x is the projection of the magnetization vector.

In order to achieve a high-contrast MOKE signal, we employed a balanced detection scheme. Using a half-wave plate ($\lambda/2$), we introduced s-polarization into the p-polarized

light. As a consequence, the p-polarized component experienced changes upon reflection from the sample due to the influence of the magnetic field, while the s-component remained unaffected by the field. A Wollaston prism separated the p- and s-components, directing them to the differential photodetector. The difference between the magnetically influenced and unaffected intensities ($\Delta I = I_{pp} - I_s$) represented our magneto-optical signal, ΔI. The reflected s-polarized light served as the reference reflectivity, proportional to I_0. The ΔI value was derived using a lock-in amplifier in sync with the magnetic field and captured using a data acquisition (DAQ) card programmed with LabVIEW. The reference value (I_0) was ascertained directly from the photodetector.

A 3D-stage was used to scan the sample point-by-point in the x and y directions (scanning MOKE or S-MOKE), as illustrated in Figure 1 (inset). Our microscope setup, consisting of a $10\times$ objective, a beam splitter, a CCD, and a diode lamp, allowed for relative positioning of the structures to the focused beam and monitoring of the scanning progress.

This setup, while acting as a 2D extension of the 1D-S-MOKE-methodology for magneto-plasmonic applications [43], underscores the role of polarization optics in our experiments. This configuration, compared to traditional methods that use a reference beam from an additional beam splitter, is both simpler and more robust, and it can be easily adapted to longitudinal and polar S-MOKE configurations.

3. Results and Discussion

In this section, we present our findings on the magnetic properties of the FeRh structures formed after laser irradiation and discuss the processes that contribute to the results. Microphotographs of the structures created by laser irradiation revealed their morphology and dimensions (Figure 2a–c). Figure 2b presents a microphotograph of the structure created after irradiation by a laser pulse with a fluence of F = 0.88 J/cm^2. At first glance, this structure appears as a dark, elliptical blotch on the original film, with diameters of 20 and 30 μm, fringed by residual remnants. The red curve in Figure 2b,c represents an AFM measurement of the relief profile within the structure, providing a more intricate understanding of its morphology. According to this analysis, the dark blotch is likely a result of laser-induced material transformation or deposition on the film surface. Comparatively, the structure created at higher fluences, as demonstrated in Figure 2c, exhibits clearer and more defined boundaries. A close inspection of the relief highlights the formation of a near 45 nm crater, which is accompanied by residues at the film base and around the crater periphery. This observation suggests the film has undergone partial removal, i.e., ablation.

Figure 2d shows the Scanning Magneto-Optical Kerr Effect (S-MOKE) map at the position previously visualized in Figure 2b. The absence of detectable signals within this map suggests that the structure retains its antiferromagnetic (AF) phase after the laser irradiation. Conversely, as demonstrated in Figure 2e, a structure with material removal showcases identifiable signals within its confines, which is indicative of a phase transition. However, the unaltered film surrounding the ablated region displays a lack of discernible signals, implying it remains in its original phase.
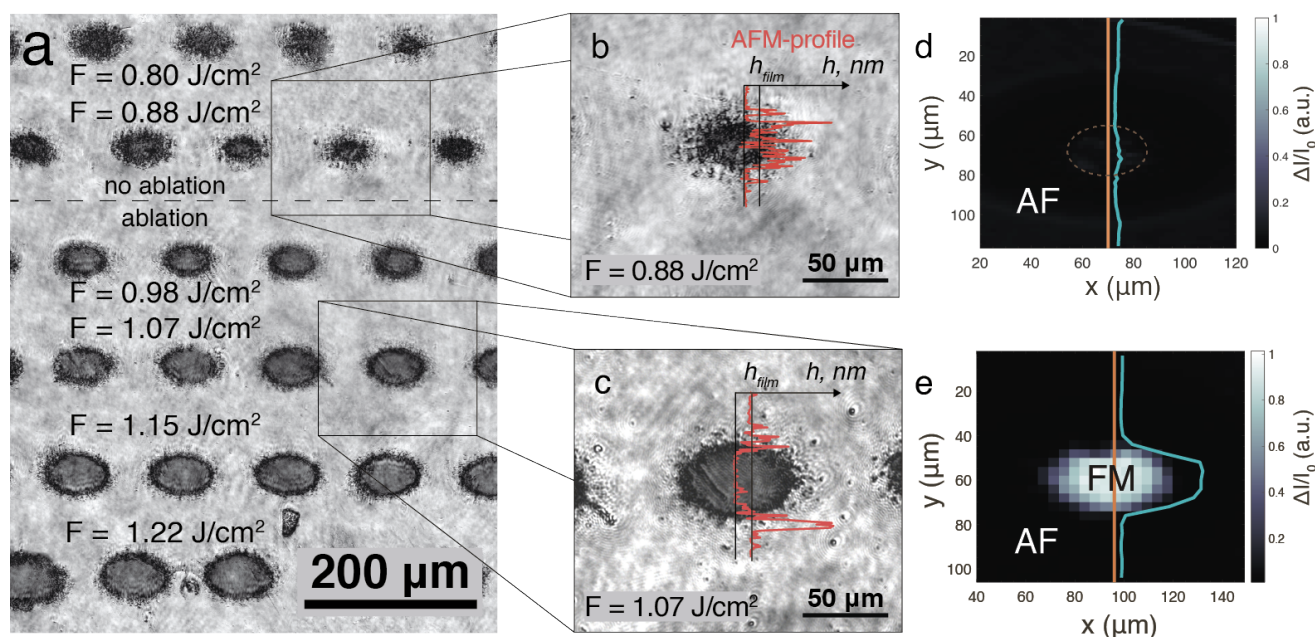
Figure 2. The microscopic pictures of the fs-laser produced structures in 45 nm thick B2-FeRh film: (**a**) Optical microscopy of the obtained structures film under F in a range from 0.8 to 1.25 J/cm^2. Optical microscopy of the structure obtained by the pulse with (**b**) F = 0.88 J/cm^2 and (**c**) F = 1.07 J/cm^2. The red curve corresponds to the topographic profile measured with AFM. h_{film} corresponds to the thickness of the film (45 nm). (**d**) S-MOKE pictures for the structures produced at the (**d**) F = 0.88 J/cm^2 and (**e**) F = 1.07 J/cm^2. The turquoise curve describes the spatial distribution of the MOKE signals obtained in the center along the orange line. AF stands for antiferromagnetic, FM stands for ferromagnetic.

In the experiments, laser irradiation exhibiting a Gaussian intensity profile was utilized to generate the structures. A specific threshold fluence is necessary to initiate the ablation process. By employing Liu's method [44], the Gaussian distribution parameters can be deduced from the pulse energy and dimensions of the structure. Consequently, a linear relationship between the radial size (r^2) of the structure and the natural logarithm of the pulse energy is established. Figure 3a demonstrates this relationship for the structures obtained with ablation, plotting r^2 against $\ln(E_{pulse})$. The intersection point of the linear relationship with the zero value represents the fluence threshold for ablation. In the case of FeRh, the threshold energy (E_{th}) is (31 ± 3) µJ, and the threshold fluence (F_{th}) is (0.92 ± 0.07) J/cm^2.

Figure 2e previously depicted the spatial distribution of the magneto-optical signal within the structure. Given that the structure was produced using a laser beam with a spatial intensity distribution, the association between the magneto-optical signal and intensity can be ascertained by comparing these two distributions.

Figure 3b demonstrates the dependence of the magneto-optical signal on the laser fluence. Up to 0.91 J/cm^2, FeRh retains its antiferromagnetic properties, exhibiting magnetization values approximating 0. Above 0.91 J/cm^2, the magneto-optical signal experiences a rapid increase, reaching its peak value of (3.8 ± 0.4) × 10^{-3} between 1.2 and 1.4 J/cm^2. Following this, a reduction to 2.9×10^{-3} occurs.

As observed in Figure 3b, the ablation threshold and the value corresponding to the phase transition from antiferromagnetic to ferromagnetic are nearly identical. This finding implies that the ablation process is the primary factor responsible for the magnetic phase transition observed in FeRh.
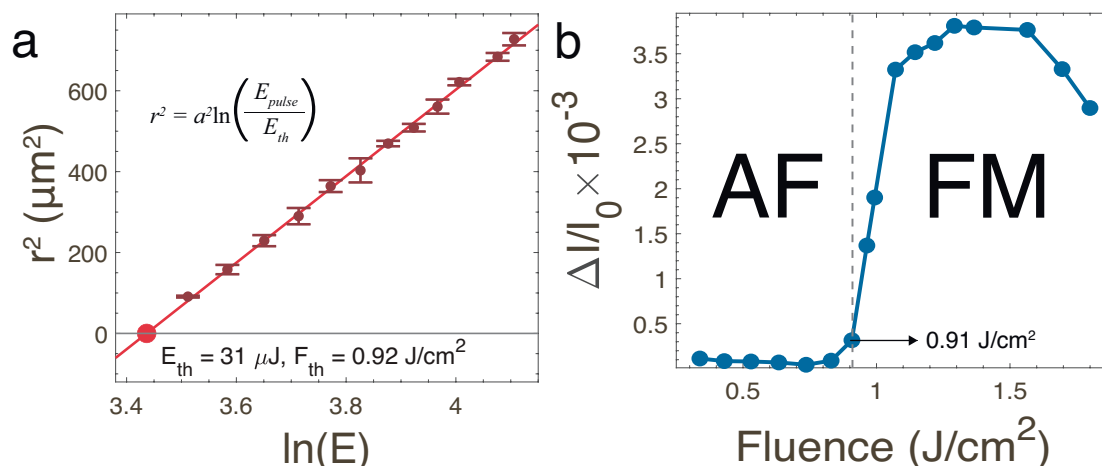
Figure 3. (**a**) Squared radius of the ablation-induced structure dependence on the natural logarithm of energy pulse (E_{pulse}). The intersection with the line y = 0 of the linear fit allows finding the threshold energy (E_{th}) and threshold fluence (F_{th}) as well according to the inserted formula [44]. (**b**) T-MOKE dependence on the fluence evaluated from the maps for each fs-laser processed structure. The lines are to guide the eye along data points.

To investigate the effect of temperature changes on the magneto-optical properties, we modified our experimental setup by incorporating an additional CW-laser from the back side of the sample during magneto-optical signal measurements (Figure 4a) at ambient atmosphere. This CW-laser, with a wavelength of around 450 nm, was focused into a 150 µm spot. By adjusting the power of the laser, the temperature of the sample could be altered, enabling the acquisition of magneto-optical signals at the selected power levels.

Figure 4b presents the results obtained for the initial FeRh film. The lower horizontal axis represents power, while the blue curve corresponds to the MOKE signal measured during sample heating. Magnetization appears at a power of approximately 0.5 W, increasing to a maximum value of $(4.6 \pm 0.4) \times 10^{-3}$ before declining and approaching 0 at 2.5 W. This behavior is consistent with the well-known FeRh phase diagram [19] and represents the consequent AF-FM and FM-PM phase transitions observed in B2-ordered FeRh [22]. Based on magnetometry tests conducted on the samples, the AF-FM phase transition occurs at 370–400 K, while the FM-PM phase transition is reached at 670 K [22]. With this information, the power scale can be converted to a relative temperature scale, as displayed on the upper horizontal axis of Figure 4b.

Following the heating of the sample to a power of 2.5 W, measurements have been continued as the power was reduced; i.e., the sample was cooled. Between 2.5 and 0.6 W, or from 670 to 390 K, the magnetization was increasing on the same trajectory, while it was decreasing under heating. However, in the temperature range of 390 to 360 K, magnetization exhibited a continuous increase, which was followed by a rapid decline after reaching its maximum value, i.e., performing the hysteresis. The magnetization eventually approached zero at approximately 350 K, which is in agreement with the magnetometry data. This observed behavior aligns with previously reported FeRh characteristics described in the literature [22,45,46].
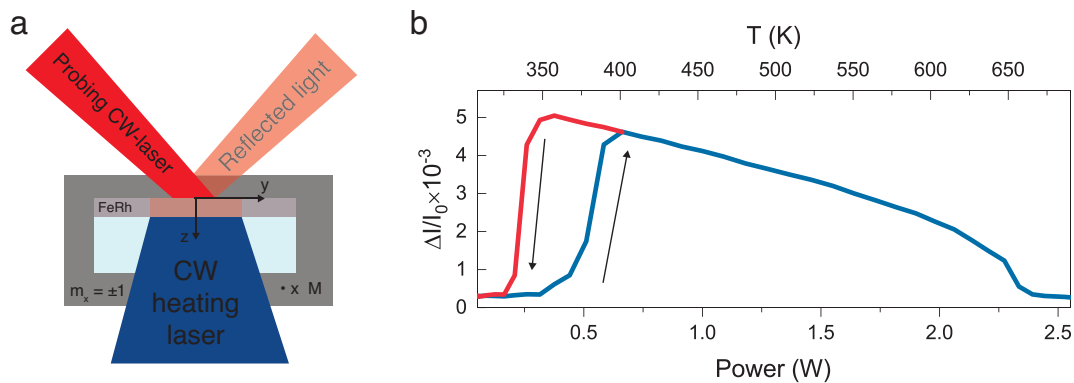
Figure 4. (**a**) Schematics of the measurements under additional heating from the back side of the film with an additional CW-laser (**b**) The results of the measurements under heating for untreated FeRh. The blue curve demonstrates the magnetic behavior during the heating phase, with increasing laser power resulting in increased film temperature, up to around 670 K (2.5 W). Upon reversing the heating process, measurements exhibit a steady response until a critical range of ∼370–390 K (0.6 W) is reached, at which point the red trajectory becomes descriptive of the observed behavior.

After examining the initial film, we turned our attention to the structures created through laser irradiation (Figure 5a). First, we carried out a spatial scan at room temperature once again, with the results shown in Figure 5b for a structure obtained at F = 1.8 J/cm^2. Following the measurements, only the surrounding area displayed the FM phase, with a width between 8 and 16 µm. No ferromagnetic properties were evident in the center of the ablated structure compared to the case before the heating of the initial film in Figure 5a, which is a trend consistent across all structures.

Subsequently, we conducted a scan along the horizontal line in the center of the structure (indicated by the red line in Figure 5b), changing the temperature at each point. Figure 5c presents the resulting data. The curved shapes of the areas can be attributed to the movement of the sample due to the applied temperature. During the temperature change, a drastic increase in magnetization was observed starting from ∼370-390 K (0.6 W), suggesting the AF-FM phase transition for the untreated FeRh.

Notably, no variation in the MOKE signal with temperature was observed inside the ablated structure. Consequently, the magnetization behavior of the laser-produced structures does not exhibit the same reversibility as the initial film.
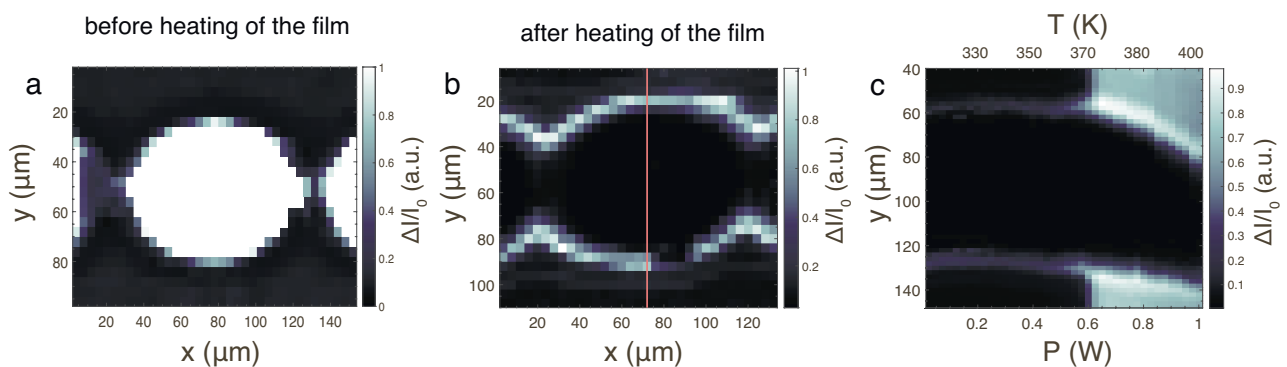
Figure 5. (**a**) S-MOKE picture taken on a laser-ablated structure in FeRh thin film obtained at F = 1.8 J/cm^2 at room temperature. (**b**) S-MOKE picture taken on a laser-ablated structure in FeRh thin film obtained at F = 1.8 J/cm^2 at room temperature after the heating with CW-laser to T > 600 K at ambient atmosphere. (**c**) The S-MOKE signal taken along the red line from the left picture (**b**) with changing the power of the heating laser (temperature) at every point. The curvature is due to a sample drift.

The correlation of the observed threshold in S-MOKE measurements with the ablation threshold invites speculation about its physical origin. The metamagnetic AF-FM phase transition in FeRh is sensitive to the composition [47], structural order [37] strain [33,48], and thickness of the film [49], which offers a variety of ways to stabilize the FM state of laser-ablated FeRh at room temperature. Experimental studies of femtosecond laser ablation clearly demonstrate that it evolves through the sequence of intermediate states characterized by low density [50]. Moreover, in the initial phase, the non-ablating part of material film is separated by an optically thick shell of laser-melted material moving away from the surface and existing on nanosecond timescales [51,52]. Both effects have been confirmed by theoretical simulations [53]. This means that the remaining part of the material, which has evolved through the low-density states, has been protected from the contact with ambient atmosphere (and thus, atmospheric pressure, oxidation and photochemistry in the liquid phase) for at least a few nanoseconds. An FM behavior in the ablated region (Figure 2e) might be a result of the combined effect of non-stoichiometry, chemical disorder and residual strains after the melting and the re-solidification during the ablation process. The sensitivity of the observed MOKE signal to the thermal annealing of the sample performed using a CW laser at ambient atmosphere can be caused by the annealing of residual stresses combined with the oxidation effects of a thin FM layer remaining at the crater of an ablated structure (Figure 2c). In contrast, the untreated area of a 45 nm thick FeRh film around the ablated crater exhibits an AF-FM phase transition when heated at the same conditions. A possible route for future experiments would be to create such structures using controlled thermo-mechanical femtosecond laser spallation by illuminating FeRh films through the substrate in the regime of closed spallation cavities [54]. Such experiments with partially melted and cavity-protected FeRh spieces are expected to shed light on the physical origin of ablation-induced phase transformation in FeRh film.

4. Conclusions

In summary, we have investigated the magnetic properties of FeRh thin films irradiated by single high-intensity femtosecond laser pulses in the ablation regime. Scanning MOKE (S-MOKE) microscopy was employed to study the magnetic phase after fs-laser processing, revealing the appearance of a magneto-optical signal at the bottom of the ablation crater. The dependence of the magneto-optical signal on the laser fluence demonstrates a strong correlation between the ablation process and the magnetic behavior in FeRh thin films. The transition from the antiferromagnetic to the ferromagnetic state in the laser-ablated regions has been observed, while the surrounding initial film retained its antiferromagnetic properties. CW-laser-assisted temperature-dependent measurements performed both on the initial film and the laser-created structures revealed that the magnetic properties of the ablated structures did not display the same reversibility as the untreated B2-ordered film. This finding suggests that laser ablation-induced phase transformation and changes in magnetic properties in FeRh thin films are irreversible when performed under ambient atmosphere. The interplay of ultrafast metamagnetic and structural phase transitions in FeRh [39,42] at elevated pump laser fluences remains the subject of future investigations.

Author Contributions: Conceptualization, P.V. (Pavel Varlamov), A.S. and V.T.; methodology, O.N., P.V. (Paolo Vavassori) and V.T.; software, P.V. (Pavel Varlamov) and A.D.N.; validation, P.V. (Pavel Varlamov) and A.D.N.; formal analysis, P.V. (Pavel Varlamov); investigation, P.V. (Pavel Varlamov) and A.D.N.; resources, Y.L., M.R., M.F., O.N. and V.T.; data curation, P.V. (Pavel Varlamov); writing—original draft preparation, P.V. (Pavel Varlamov); writing—review and editing, P.V. (Pavel Varlamov), A.S., P.V. (Paolo Vavassori) and V.T.; visualization, P.V. (Pavel Varlamov); supervision, M.R., M.F., O.N., P.V. (Paolo Vavassori) and V.T.; project administration, P.V. (Paolo Vavassori) and V.T.; funding acquisition, M.R., M.F., A.S., P.V. (Paolo Vavassori) and V.T. All authors have read and agreed to the published version of the manuscript.

Institutional Review Board Statement: Not applicable.

Informed Consent Statement: Not applicable.

Data Availability Statement: The data is available from the authors upon reasonable request.

Conflicts of Interest: The authors declare no conflict of interest.

References

1. Crangle, J.; Goodman, G. The magnetization of pure iron and nickel. *Proc. R. Soc. London. A. Math. Phys. Sci.* **1971**, *321*, 477–491.
2. Beaurepaire, E.; Merle, J.C.; Daunois, A.; Bigot, J.Y. Ultrafast spin dynamics in ferromagnetic nickel. *Phys. Rev. Lett.* **1996**, *76*, 4250. [CrossRef]
3. Van Kampen, M.; Jozsa, C.; Kohlhepp, J.T.; LeClair, P.; Lagae, L.; De Jonge, W.J.M.; Koopmans, B. All-optical probe of coherent spin waves. *Phys. Rev. Lett.* **2002**, *88*, 227201. [CrossRef] [PubMed]
4. Bigot, J.Y.; Vomir, M.; Andrade, L.H.F.; Beaurepaire, E. Ultrafast magnetization dynamics in ferromagnetic cobalt: The role of the anisotropy. *Chem. Phys.* **2005**, *318*, 137–146. [CrossRef]
5. Salikhov, R.; Alekhin, A.; Parpiiev, T.; Pezeril, T.; Makarov, D.; Abrudan, R.; Meckenstock, R.; Radu, F.; Farle, M.; Zabel, H.; et al. Gilbert damping in NiFeGd compounds: Ferromagnetic resonance versus time-resolved spectroscopy. *Phys. Rev. B* **2019**, *99*, 104412. [CrossRef]
6. Scherbakov, A.V.; Salasyuk, A.S.; Akimov, A.V.; Liu, X.; Bombeck, M.; Brüggemann, C.; Yakovlev, D.R.; Sapega, V.F.; Furdyna, J.K.; Bayer, M. Coherent magnetization precession in ferromagnetic (Ga, Mn) As induced by picosecond acoustic pulses. *Phys. Rev. Lett.* **2010**, *105*, 117204. [CrossRef]
7. Kim, J.W.; Vomir, M.; Bigot, J.Y. Ultrafast magnetoacoustics in nickel films. *Phys. Rev. Lett.* **2012**, *109*, 166601. [CrossRef]
8. Vlasov, V.S.; Golov, A.V.; Kotov, L.N.; Shcheglov, V.I.; Lomonosov, A.M.; Temnov, V.V. The modern problems of ultrafast magnetoacoustics. *Acoust. Phys.* **2022**, *68*, 18–47. [CrossRef]
9. Kimel, A.; Zvezdin, A.; Sharma, S.; Shallcross, S.; De Sousa, N.; García-Martín, A.; Salvan, G.; Hamrle, J.; Stejskal, O.; McCord, J.; et al. The 2022 magneto-optics roadmap. *J. Phys. D Appl. Phys.* **2022**, *55*, 463003. [CrossRef]
10. Kisielewski, J.; Kurant, Z.; Sveklo, I.; Tekielak, M.; Wawro, A.; Maziewski, A. Magnetic phases in Pt/Co/Pt films induced by single and multiple femtosecond laser pulses. *J. Appl. Phys.* **2016**, *119*, 193901. [CrossRef]
11. Urner-Wille, M.; Kobs, R.; Witter, K. Picosecond laser-induced change of the magnetic properties of amorphous GdFeBi-films. *IEEE Trans. Magn.* **1981**, *17*, 2621–2623. [CrossRef]
12. Ehrler, J.; He, M.; Shugaev, M.V.; Polushkin, N.I.; Wintz, S.; Liersch, V.; Cornelius, S.; Hübner, R.; Potzger, K.; Lindner, J.; et al. Laser-rewriteable ferromagnetism at thin-film surfaces. *ACS Appl. Mater. Interfaces* **2018**, *10*, 15232–15239. [CrossRef] [PubMed]
13. Polushkin, N.I.; Oliveira, V.; Vilar, R.; He, M.; Shugaev, M.V.; Zhigilei, L.V. Phase-change magnetic memory: Rewritable ferromagnetism by laser quenching of chemical disorder in $Fe_{60}Al_{40}$ alloy. *Phys. Rev. Appl.* **2018**, *10*, 024023. [CrossRef]
14. Bali, R.; Wintz, S.; Meutzner, F.; Hübner, R.; Boucher, R.; Ünal, A.A.; Valencia, S.; Neudert, A.; Potzger, K.; Bauch, J.; et al. Printing nearly-discrete magnetic patterns using chemical disorder induced ferromagnetism. *Nano Lett.* **2014**, *14*, 435–441. [CrossRef]
15. Strusch, T.; Lenz, K.; Meckenstock, R.; Bali, R.; Ehrler, J.; Lindner, J.; Fassbender, J.; Farle, M.; Potzger, K.; Semisalova, A. Spin pumping at interfaces with ferro-and paramagnetic $Fe_{60}Al_{40}$ films acting as spin source and spin sink. *J. Appl. Phys.* **2022**, *132*, 213906. [CrossRef]
16. Stanciu, C.D.; Hansteen, F.; Kimel, A.V.; Kirilyuk, A.; Tsukamoto, A.; Itoh, A.; Rasing, T. All-optical magnetic recording with circularly polarized light. *Phys. Rev. Lett.* **2007**, *99*, 047601. [CrossRef]
17. Vahaplar, K.; Kalashnikova, A.M.; Kimel, A.V.; Gerlach, S.; Hinzke, D.; Nowak, U.; Chantrell, R.; Tsukamoto, A.; Itoh, A.; Kirilyuk, A.; et al. All-optical magnetization reversal by circularly polarized laser pulses: Experiment and multiscale modeling. *Phys. Rev. B* **2012**, *85*, 104402. [CrossRef]
18. Ostler, T.A.; Barker, J.; Evans, R.F.L.; Chantrell, R.W.; Atxitia, U.; Chubykalo-Fesenko, O.; El Moussaoui, S.; Le Guyader, L.; Mengotti, E.; Heyderman, L.J.; et al. Ultrafast heating as a sufficient stimulus for magnetization reversal in a ferrimagnet. *Nat. Commun.* **2012**, *3*, 666. [CrossRef]
19. Lewis, L.H.; Marrows, C.H.; Langridge, S. Coupled magnetic, structural, and electronic phase transitions in FeRh. *J. Phys. D Appl. Phys.* **2016**, *49*, 323002. [CrossRef]
20. Griggs, W.; Eggert, B.; Liedke, M.O.; Butterling, M.; Wagner, A.; Kentsch, U.; Hirschmann, E.; Grimes, M.; Caruana, A.J.; Kinane, C.; et al. Depth selective magnetic phase coexistence in FeRh thin films. *APL Mater.* **2020**, *8*, 121103. [CrossRef]

21. Nadarajah, R.; Tahir, S.; Landers, J.; Koch, D.; Semisalova, A.S.; Wiemeler, J.; El-Zoka, A.; Kim, S.H.; Utzat, D.; Möller, R.; et al. Controlling the oxidation of magnetic and electrically conductive solid-solution iron-rhodium nanoparticles synthesized by laser ablation in liquids. *Nanomaterials* **2020**, *10*, 2362. [CrossRef]

22. Heidarian, A.; Stienen, S.; Semisalova, A.; Yuan, Y.; Josten, E.; Hübner, R.; Salamon, S.; Wende, H.; Gallardo, R.; Grenzer, J.; et al. Ferromagnetic resonance of MBE-grown FeRh thin films through the metamagnetic phase transition. *Phys. Status Solidi* **2017**, *254*, 1700145. [CrossRef]

23. Eggert, B.; Schmeink, A.; Lill, J.; Liedke, M.O.; Kentsch, U.; Butterling, M.; Wagner, A.; Pascarelli, S.; Potzger, K.; Lindner, J.; et al. Magnetic response of FeRh to static and dynamic disorder. *RSC Adv.* **2020**, *10*, 14386–14395. [CrossRef]

24. Vogler, C.; Abert, C.; Bruckner, F.; Suess, D. Noise Reduction Based on an Fe- Rh Interlayer in Exchange-Coupled Heat-Assisted Recording Media. *Phys. Rev. Appl.* **2017**, *8*, 054021. [CrossRef]

25. Feng, Z.; Yan, H.; Liu, Z. Electric-Field Control of Magnetic Order: From FeRh to Topological Antiferromagnetic Spintronics. *Adv. Electron. Mater.* **2019**, *5*, 1800466. [CrossRef]

26. Qiao, K.; Liang, Y.; Zhang, H.; Hu, F.; Yu, Z.; Long, Y.; Wang, J.; Sun, J.; Zhao, T.; Shen, B. Manipulation of magnetocaloric effect in FeRh films by epitaxial growth. *J. Alloys Compd.* **2022**, *907*, 164574. [CrossRef]

27. Vieira, R.M.; Eriksson, O.; Bergman, A.; Herper, H.C. High-throughput compatible approach for entropy estimation in magnetocaloric materials: FeRh as a test case. *J. Alloys Compd.* **2021**, *857*, 157811. [CrossRef]

28. Chirkova, A.; Skokov, K.P.; Schultz, L.; Baranov, N.V.; Gutfleisch, O.; Woodcock, T.G. Giant adiabatic temperature change in FeRh alloys evidenced by direct measurements under cyclic conditions. *Acta Mater.* **2016**, *106*, 15–21. [CrossRef]

29. Bennett, S.P.; Ambaye, H.; Lee, H.; LeClair, P.; Mankey, G.J.; Lauter, V. Direct evidence of anomalous interfacial magnetization in metamagnetic Pd doped FeRh thin films. *Sci. Rep.* **2015**, *5*, 9142. [CrossRef] [PubMed]

30. Hu, Q.B.; Li, J.; Wang, C.C.; Zhou, Z.J.; Cao, Q.Q.; Zhou, T.J.; Wang, D.H.; Du, Y.W. Electric field tuning of magnetocaloric effect in FeRh$_{0.96}$Pd$_{0.04}$/PMN-PT composite near room temperature. *Appl. Phys. Lett.* **2017**, *110*, 222408. [CrossRef]

31. Barua, R.; Jiménez-Villacorta, F.; Lewis, L.H. Predicting magnetostructural trends in FeRh-based ternary systems. *Appl. Phys. Lett.* **2013**, *103*, 102407. [CrossRef]

32. Urban, C.; Bennett, S.P.; Schuller, I.K. Hydrostatic pressure mapping of barium titanate phase transitions with quenched FeRh. *Sci. Rep.* **2020**, *10*, 6312. [CrossRef] [PubMed]

33. Fina, I.; Fontcuberta, J. Strain and voltage control of magnetic and electric properties of FeRh films. *J. Phys. D Appl. Phys.* **2019**, *53*, 023002. [CrossRef]

34. Fujita, N.; Matsui, T.; Kosugi, S.; Satoh, T.; Saitoh, Y.; Takano, K.; Koka, M.; Kamiya, T.; Seki, S.; Iwase, A. Micrometer-sized magnetic patterning of FeRh films using an energetic ion microbeam. *Jpn. J. Appl. Phys.* **2010**, *49*, 060211. [CrossRef]

35. Koide, T.; Satoh, T.; Kohka, M.; Saitoh, Y.; Kamiya, T.; Ohkouchi, T.; Kotsugi, M.; Kinoshita, T.; Nakamura, T.; Iwase, A.; et al. Magnetic patterning of FeRh thin films by energetic light ion microbeam irradiation. *Jpn. J. Appl. Phys.* **2014**, *53*, 05FC06. [CrossRef]

36. Heidarian, A.; Bali, R.; Grenzer, J.; Wilhelm, R.A.; Heller, R.; Yildirim, O.; Lindner, J.; Potzger, K. Tuning the antiferromagnetic to ferromagnetic phase transition in FeRh thin films by means of low-energy/low fluence ion irradiation. *Nucl. Instruments Methods Phys. Res. Sect. B Beam Interact. Mater. Atoms* **2015**, *358*, 251–254. [CrossRef]

37. Bennett, S.P.; Herklotz, A.; Cress, C.D.; Ievlev, A.; Rouleau, C.M.; Mazin, I.I.; Lauter, V. Magnetic order multilayering in FeRh thin films by He-Ion irradiation. *Mater. Res. Lett.* **2018**, *6*, 106–112. [CrossRef]

38. Cress, C.D.; Wickramaratne, D.; Rosenberger, M.R.; Hennighausen, Z.; Callahan, P.G.; LaGasse, S.W.; Bernstein, N.; van 't Erve, O.M.; Jonker, B.T.; Qadri, S.B.; et al. Direct-Write of Nanoscale Domains with Tunable Metamagnetic Order in FeRh Thin Films. *ACS Appl. Mater. Interfaces* **2021**, *13*, 836–847. [CrossRef]

39. Ju, G.; Hohlfeld, J.; Bergman, B.; van de Veerdonk, R.J.M.; Mryasov, O.N.; Kim, J.Y.; Wu, X.; Weller, D.; Koopmans, B. Ultrafast generation of ferromagnetic order via a laser-induced phase transformation in FeRh thin films. *Phys. Rev. Lett.* **2004**, *93*, 197403. [CrossRef]

40. Bergman, B.; Ju, G.; Hohlfeld, J.; van de Veerdonk, R.J.M.; Kim, J.Y.; Wu, X.; Weller, D.; Koopmans, B. Identifying growth mechanisms for laser-induced magnetization in FeRh. *Phys. Rev. B* **2006**, *73*, 060407. [CrossRef]

41. Pressacco, F.; Uhlíř, V.; Gatti, M.; Nicolaou, A.; Bendounan, A.; Arregi, J.A.; Patel, S.K.K.; Fullerton, E.E.; Krizmancic, D.; Sirotti, F. Laser induced phase transition in epitaxial FeRh layers studied by pump-probe valence band photoemission. *Struct. Dyn.* **2018**, *5*, 034501. [CrossRef]

42. Awari, N.; Semisalova, A.; Deinert, J.C.; Lenz, K.; Lindner, J.; Fullerton, E.; Uhlíř, V.; Li, J.; Clemens, B.; Carley, R.; et al. Monitoring laser-induced magnetization in FeRh by transient terahertz emission spectroscopy. *Appl. Phys. Lett.* **2020**, *117*, 122407. [CrossRef]

43. Temnov, V.V.; Armelles, G.; Woggon, U.; Guzatov, D.; Cebollada, A.; Garcia-Martin, A.; Garcia-Martin, J.M.; Thomay, T.; Leitenstorfer, A.; Bratschitsch, R. Active magneto-plasmonics in hybrid metal–ferromagnet structures. *Nat. Photonics* **2010**, *4*, 107–111. [CrossRef]

44. Liu, J.M. Simple technique for measurements of pulsed Gaussian-beam spot sizes. *Opt. Lett.* **1982**, *7*, 196–198. [CrossRef] [PubMed]

45. Dróżdż, P.; Ślęzak, M.; Matlak, K.; Kozioł-Rachwał, A.; Korecki, J.; Slezak, T. Spin-flop coupling induced large coercivity enhancement in Fe/FeRh/W(110) bilayers across ferromagnetic–antiferromagnetic phase transition of FeRh alloy. *J. Magn. Magn. Mater.* **2020**, *498*, 166258. [CrossRef]

46. Xie, Y.; Zhan, Q.; Shang, T.; Yang, H.; Liu, Y.; Wang, B.; Li, R.W. Electric field control of magnetic properties in FeRh/PMN-PT heterostructures. *AIP Adv.* **2018**, *8*, 055816. [CrossRef]

47. Staunton, J.B.; Banerjee, R.; Dias, M.d.S.; Deak, A.; Szunyogh, L. Fluctuating local moments, itinerant electrons, and the magnetocaloric effect: Compositional hypersensitivity of FeRh. *Phys. Rev. B* **2014**, *89*, 054427. [CrossRef]

48. Arregi, J.A.; Caha, O.; Uhlíř, V. Evolution of strain across the magnetostructural phase transition in epitaxial FeRh films on different substrates. *Phys. Rev. B* **2020**, *101*, 174413. [CrossRef]

49. Barton, C.W.; Ostler, T.A.; Huskisson, D.; Kinane, C.J.; Haigh, S.J.; Hrkac, G.; Thomson, T. Substrate induced strain field in FeRh epilayers grown on single crystal MgO (001) substrates. *Sci. Rep.* **2017**, *7*, 44397. [CrossRef]

50. Temnov, V.V. *Ultrafast Laser-Induced Phenomena in Solids Studied by Time-Resolved Interferometry*; University of Duisburg-Essen: Duisburg, Germany, 2004.

51. Sokolowski-Tinten, K.; Bialkowski, J.; Cavalleri, A.; von der Linde, D.; Oparin, A.; Meyer-ter-Vehn, J.; Anisimov, S.I. Transient states of matter during short pulse laser ablation. *Phys. Rev. Lett.* **1998**, *81*, 224. [CrossRef]

52. Temnov, V.V.; Sokolowski-Tinten, K.; Zhou, P.; von der Linde, D. Ultrafast imaging interferometry at femtosecond-laser-excited surfaces. *JOSA B* **2006**, *23*, 1954–1964. [CrossRef]

53. Ivanov, D.S.; Zhigilei, L.V. Combined atomistic-continuum modeling of short-pulse laser melting and disintegration of metal films. *Phys. Rev. B* **2003**, *68*, 064114. [CrossRef]

54. Temnov, V.V.; Alekhin, A.; Samokhvalov, A.; Ivanov, D.S.; Lomonosov, A.; Vavassori, P.; Modin, E.; Veiko, V.P. Nondestructive femtosecond laser lithography of Ni nanocavities by controlled thermo-mechanical spallation at the nanoscale. *Nano Lett.* **2020**, *20*, 7912–7918. [CrossRef] [PubMed]